The Journal of Chemical Physics

Proton tunneling in a two-dimensional potential energy surface with a non-linear system–bath interaction: Thermal suppression of reaction rate

Cite as: J. Chem. Phys. **152**, 214114 (2020); https://doi.org/10.1063/5.0010580
Submitted: 13 April 2020 . Accepted: 14 May 2020 . Published Online: 04 June 2020

Jiaji Zhang, Raffaele Borrelli, and Yoshitaka Tanimura

The Journal of Chemical Physics ARTICLE scitation.org/journal/jcp

Proton tunneling in a two-dimensional potential energy surface with a non-linear system–bath interaction: Thermal suppression of reaction rate

Cite as: J. Chem. Phys. 152, 214114 (2020); doi: 10.1063/5.0010580
Submitted: 13 April 2020 • Accepted: 14 May 2020 •
Published Online: 4 June 2020

Jiaji Zhang,[1,a] Raffaele Borrelli,[2,b] and Yoshitaka Tanimura[1,c]

AFFILIATIONS

[1] Department of Chemistry, Graduate School of Science, Kyoto University, Kyoto 606-8502, Japan
[2] DISAFA, University of Torino, Largo Paolo Braccini 2, I-10095 Grugliasco, Italy

[a] Electronic mail: zhang.jiaji.84e@st.kyoto-u.ac.jp
[b] Electronic mail: raffaele.borrelli@unito.it
[c] Author to whom correspondence should be addressed: tanimura.yoshitaka.5w@kyoto-u.jp

ABSTRACT

We consider a proton transfer (PT) system described by a proton transfer reaction (PTR) coordinate and a rate promoting vibrational (RPV) coordinate interacting with a non-Markovian heat bath. While dynamics of PT processes has been widely discussed using two-dimensional potential energy surfaces, the role of the heat bath, in particular, in a realistic form of the system–bath interaction has not been well explored. Previous studies are largely based on a one-dimensional model and linear-linear system–bath interaction. In the present study, we introduce an exponential-linear (EL) system–bath interaction, which is derived from the analysis of a PTR–RPV system in a realistic situation. This interaction mainly causes vibrational dephasing in the PTR mode and population relaxation in the RPV mode. Numerical simulations were carried out using the hierarchical equations of motion approach. We analyze the role of the heat bath interaction in the chemical reaction rate as a function of the system–bath coupling strength at different temperatures and for different values of the bath correlation time. A prominent feature of the present result is that while the reaction rate predicted from classical and quantum Kramers theory increases as the temperature increases, the present EL interaction model exhibits opposite temperature dependence. The Kramers turn-over profile of the reaction rate as a function of the system–bath coupling is also suppressed in the present EL model, turning into a plateau-like curve for larger system–bath interaction strength. Such features arise from the interplay of the vibrational dephasing process in the PTR mode and the population relaxation process in the RPV mode.

I. INTRODUCTION

Proton transfer (PT) processes play an essential role in many types of biological and functional molecular materials and determine the efficiency of the mechanisms for utilizing chemical and solar energies.[1–7] One of the central questions in the PT problem is how thermal effects, most typically fluctuation and dissipation that arise from a molecular environment (a heat bath), influence the efficiency of the PT reaction.

This problem has been a subject of open quantum dynamics theory because the PT involves a deep tunneling process that requires full quantum mechanical description of the system and because the PT system undergoes irreversible dynamics through interactions with an environment, for example, a solvent, a protein scaffold, or a nanostructured material, in a non-Markovian and non-perturbative manner.

Several theoretical approaches have been developed to account for quantum effects of chemical reactions,[8–12] but the capability to treat deep tunneling problems from such approaches is limited. Moreover, many investigations have been limited to systems defined in a one-dimensional configuration space linearly coupled with the Markovian heat bath.[13–20] In realistic situations, the potential energy surface (PES) of the PT system is defined at least in a two-dimensional configuration space, which consists of a proton transfer reaction (PTR) mode and a rate promoting vibrational (RPV) mode that comprises mostly a stretching vibration of the

hydrogen-bridged moieties. Furthermore, the system–bath interaction can be highly non-linear, which causes a strong vibrational dephasing effect on the system dynamics.

While the importance of the RPV modes has been discussed intensively,[21–23] the majority of treatments have ignored quantum mechanically entangled environmental effects, assuming static potential or employing adiabatic approximation under external perturbation.[24–28] In a realistic situation, however, proton transfer processes are controlled by transition distance and energy barrier height as a function of the RPV coordinate that is further coupled to the environmental degrees of freedom. The key aspect is that the system–bath interaction in the PT process is non-Markovian and has to be treated non-perturbatively at full quantum mechanical levels, while most of the existing theories cannot treat this effect accurately.[4,29–33]

Meanwhile, from the investigation of exciton transfer processes in photosynthetic antenna systems, it has been realized that the non-Markovian and non-perturbative system–bath interaction in quantum regime plays a central role in determining the efficiency of the exciton transition rate.[34–37] Similar to the exciton transfer problems, it is expected that the quantum nature of the system–bath interaction is also essential in determining the efficiency of the PT reaction.

In this paper, we give an extension of PT theory focusing on the role of a realistic system–bath interaction to help in further development of the investigation in this area. We consider a PT system, which is described as a two-dimensional potential coupled to the environment at finite temperature. More specifically, we consider an exponential form of the system–bath interaction that includes a RPV–bath coupling term to describe the thermal effect of the RPV mode. Employing the exact hierarchical equations of motion (HEOM) theory, we numerically simulate the PT process for different system–bath coupling strengths and noise correlation time and at different temperatures.

The organization of this paper is as follows. In Sec. II, we present a model system for the proton transfer process. Then, we show how the chemical reaction rate can be calculated from the HEOM on the basis of the linear response theory. In Sec. III, we present the numerical results and discussion, and the conclusion is given in Sec. IV.

II. THEORY

A. The system–bath Hamiltonian

We consider a proton transfer (PT) system described by PTR and rate promoting vibrational (RPV) coordinate modes. While we can treat more than three-dimensional configuration space using the energy eigenstate representations of the system, for the sake of conciseness, here we consider the two-dimensional case as a minimal model for the PT process. In our model, the potential energy surface (PES) is modulated by an environment (bath) representing the other non-RPV modes, which might represent any type of solvation or protein modes.

The system Hamiltonian is then expressed in the form

$$\hat{H}_S(\{\hat{x}_j\}) = \frac{\hat{p}^2}{2m} + \frac{\hat{P}^2}{2M} + U(\hat{q},\hat{R};\{\hat{x}_j\}). \tag{1}$$

Here, $\hat{q}$, $\hat{p}$, and m represent the coordinate, momentum, and mass of the PTR coordinate, $\hat{R}$, $\hat{P}$, and M represent those of the RPV mode, and $\{\hat{x}_j\}$ are the coordinates of the bath modes. In the above form, H_S includes the modulation of the system parameters induced by the bath coordinates.

The potential $U(\hat{q},\hat{R};\{\hat{x}_j\})$ is written as

$$U(\hat{q},\hat{R};\{\hat{x}_j\}) = D_0\left(1 - e^{-\alpha(\{\hat{x}_j\})(\hat{R}/2-\hat{q}-q_e)}\right)^2 + D_0\left(1 - e^{-\alpha(\{\hat{x}_j\})(\hat{R}/2+\hat{q}-q_e)}\right)^2 + \frac{1}{2}D_k(\hat{R}-R_e)^2, \tag{2}$$

where D_0 is the dissociation energy, q_e is the equilibrium distance of the proton, $\alpha(\{x_j\})$ is the curvature of Morse potential, which depends on the bath degrees of freedom $\{x_j\}$ (see below), D_k is the force constant for the RPV mode, and R_e is the equilibrium distance between the donor and the acceptor without the presence of the proton.

This form of the two-dimensional potential of a hydrogen-bridged system has been successfully used in the past to model hydrogen bond dynamics and spectroscopy.[38–40] The unique feature of the present model is that the effect of the environment is included via the dependence of the anharmonicity parameter α on the bath coordinates. The rationale behind this choice is that, in the above potential energy, both the height of the barrier for the proton tunneling and the vibrational frequency of the H-bond depend linearly on the α parameter. Furthermore, as we will shortly demonstrate, this type of coupling enables us to include a linear coupling between the RPV mode and the bath.

The α parameter of the potential is considered to be linearly dependent on the coordinates $\{x_j\}$ as $\alpha(\{x_j\}) = \alpha_0 + \alpha^{(1)}\sum_j g_j\hat{x}_j$, where α_0 and $\alpha^{(1)}$ are the constants that represent the curvature of the system-potential and the strength of the coupling between the system and the environment. Finally, by expanding the PES in the power series around $\{x_j\} = 0$, we obtain

$$U(\hat{q},\hat{R};\{x_j\}) = U_0(\hat{q},\hat{R}) + V(\hat{q},\hat{R})\sum_j g_j\hat{x}_j, \tag{3}$$

where $U_0(\hat{q},\hat{R}) \equiv U(\hat{q},\hat{R};\{\hat{x}_j = 0\})$ is the hydrogen bridge potential without the bath interaction (see Fig. 1) and the interaction potential $V(\hat{q},\hat{R})$ is expressed as

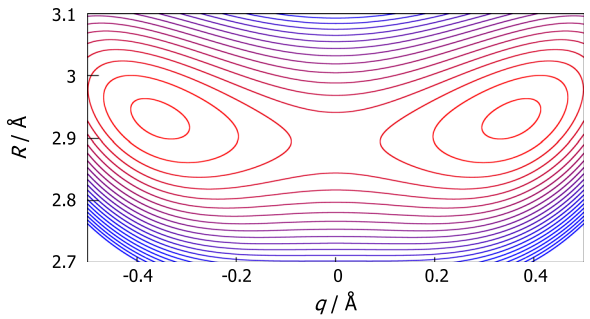

FIG. 1. Two-dimensional potential energy surface $U_0(\hat{q},\hat{R})$. The parameters of the model are reported in Table I. Contour lines are drawn every 500 cm^{-1}.

$$V(\hat{q},\hat{R}) = V_0(\hat{R}-2q_e) - V_0 e^{-\alpha_0(\hat{R}/2-q_e)} \times \left[(\hat{R}-2q_e)\cosh(\alpha_0\hat{q}) - 2\hat{q}\sinh(\alpha_0\hat{q})\right], \quad (4)$$

where $V_0 = \alpha^{(1)} D_0$. Following the standard approach of the theory of open quantum systems, we assume that the bath modes are represented by a set of harmonic oscillators, with the jth bath oscillator possessing the frequency ω_j, mass m_j, position coordinate $\hat{x}_j$, and momentum $\hat{p}_j$. The total Hamiltonian is then expressed as

$$\hat{H}_{\rm tot} = \hat{H}_S + \sum_j \left[\frac{\hat{p}_j^2}{2m_j} + \frac{1}{2}m_j\omega_j^2\left(\hat{x}_j - \frac{g_j\hat{V}(\hat{q},\hat{R})}{m_j\omega_j^2}\right)^2\right], \quad (5)$$

where $\hat{H}_S$ is the system Hamiltonian for the potential $U_0(\hat{q},\hat{R})$ and we included the counter term in the system–bath interaction.[41–43] Hereafter, we refer to $\hat{V}(\hat{q},\hat{R})\sum_j g_j\hat{x}_j$ as the exponential-linear (EL) interaction due to the form of the operator $\hat{V}$. The EL interaction mainly modulates the barrier height of the proton potential, which can be used to investigate the non-polarizable solvent effect of a realistic PTR process.[44,45] The heat bath is characterized by the spectral distribution function (SDF), defined by $J(\omega) \equiv \sum \hbar g_j^2\delta(\omega-\omega_j)/2m_j\omega_j$, and the inverse temperature, $\beta \equiv 1/k_{\rm B}T$, where $k_{\rm B}$ is the Boltzmann constant. By adjusting the form of the SDF, the properties of the local environment, for example, solvates and protein molecules, can be modeled. Typically, the SDF is estimated from linear and nonlinear infrared and Raman spectra, both experimentally[46–48] and numerically.[49–53]

The main features of the EL interaction can be illustrated by expanding $V(\hat{q},\hat{R})$ in the Taylor series with respect to $\hat{q}$ and $\hat{R}$ as

$$\hat{V}(\hat{q},\hat{R}) = \hat{V}^{(2,0)}\hat{q}^2 + \hat{V}^{(0,1)}\hat{R} + \hat{V}^{(2,1)}\hat{q}^2\hat{R} + \cdots, \quad (6)$$

where $\hat{V}^{(k,l)} = \partial^{k+l}\hat{V}/\partial\hat{q}^k\partial\hat{R}^l|_{\hat{q}=\hat{R}=0}$. It should be noted that, due to the symmetry of the potential along the proton coordinate, $V(\hat{q},\hat{R})$ is an even function of the proton coordinate $\hat{q}$. Thus, the leading order of the EL model for the PTR mode is the square-linear (SL) interaction, expressed as $\hat{q}^2\sum_j g_j x_j$, while that for the RPV mode is the linear-linear (LL) interaction, expressed as $\hat{R}\sum_j g_j x_j$. The distinct feature of the present model arises from this SL interaction in the PTR mode, while most of the system–bath models employed in the former investigations were assumed to have the LL system–bath interaction.

Although the SL interaction has been used to analyze the effects of vibrational dephasing in linear spectroscopy[54–57] as well as in ultrafast nonlinear spectroscopy,[58,59] the relevance of such an interaction has not been properly addressed in the PTR problem. We notice that our model also includes a linear coupling of the RPV mode, which has been found to be quite significant in molecular dynamics simulation of hydrogen atom transfer.[60]

In order to calculate the reaction rate, we employ the eigenstate representation for both $\hat{H}_S$ and $\hat{V}(\hat{q},\hat{R})$ (see Appendix A).

B. The reduced hierarchical equations of motion formalism

In the framework of the system–bath Hamiltonian, the characteristic feature of the environment is determined by the choice of the SDF. A typically employed SDF for a molecular environment is the Drude SDF,[41–43,61–67] the Brownian SDF,[68,69] the Ohmic SDF,[70] and their combinations.[50,71,73]

Here, we consider the Drude SDF defined by

$$J(\omega) = \frac{\hbar\zeta}{\pi}\frac{\gamma^2\omega}{\gamma^2+\omega^2}, \quad (7)$$

where the parameter γ represents the width of the spectral distribution of the collective bath modes and is the reciprocal of the noise correlation time induced by the heat bath, $\tau_c = 1/\gamma$. The parameter ζ is the system–bath coupling strength, which represents the magnitude of fluctuations and dissipations. The heat bath effect is characterized by the noise correlation function, $C(t) \equiv \langle\hat{X}_k(t)\hat{X}(0)\rangle$, which can be further expressed as a linear combination of exponential functions and a delta function, $C(t) = \sum_k (c_k' + ic_k'')\gamma_k e^{-\gamma_k|t|} + 2c_\delta\cdot\delta_t$.[61–64] Then, using the path integral method, reduced hierarchical equations of motion (HEOM) can be derived as[61–67]

$$\frac{\partial}{\partial t}\hat{\rho}_{\vec{n}}(t) = -\left[\frac{i}{\hbar}\hat{\mathcal{L}}_S + \sum_{k=1}^K n_k\gamma_k + c_\delta\hat{\Phi}^2\right]\hat{\rho}_{\vec{n}}(t) - \hat{\Phi}\sum_{k=1}^K\hat{\rho}_{\vec{n}+\vec{e}_k}(t) - \sum_{k=1}^K n_k\hat{\Theta}_k\hat{\rho}_{\vec{n}-\vec{e}_k}(t), \quad (8)$$

where we introduce the operators $\hat{\mathcal{L}}_S\hat{\rho} \equiv [\hat{H}_S,\hat{\rho}]$, $\hat{\Phi}\hat{\rho} \equiv (i/\hbar)[\hat{V},\hat{\rho}]$, $\hat{\Psi}\hat{\rho} \equiv (1/\hbar)\{\hat{V},\hat{\rho}\}$, and $\hat{\Theta}_k \equiv c_k'\hat{\Phi} - c_k''\hat{\Psi}$. The vector $\vec{e}_k$ is the unit vector along the kth direction. The HEOM consist of an infinite number of equations. These equations can be truncated at finite order when $\sum_k n_k$ first exceeds a properly chosen large value N.[63]

C. Flux–flux correlation function: Chemical reaction rate

A chemical reaction process is typically characterized by a rate constant defined by the flux–flux correlation (FFC) function.[2,74,75,77] In this paper, we consider the time dependent rate constant, which is defined in terms of the canonical correlation function as[75]

$$k(t) = \frac{1}{\beta}\int_0^\beta d\lambda\,{\rm Tr}\left\{\hat{\rho}_{\rm tot}^{\rm eq}e^{\lambda\hat{H}_{\rm tot}}\dot{\hat{\theta}}_R e^{-\lambda\hat{H}_{\rm tot}}\dot{\hat{\theta}}_R(t)\right\} \equiv \int_0^t dt\left\langle\dot{\hat{\theta}}_R;\dot{\hat{\theta}}_R(t)\right\rangle, \quad (9)$$

where $\hat{\theta}_R$ is the projection operator introduced to evaluate the population of the reactant and $\dot{\hat{\theta}}_R = [\hat{\theta}_R,\hat{H}_{\rm tot}]/i\hbar$. Typically, $\hat{\theta}_R$ is chosen to be the Heaviside step function of the proton coordinate q.[75] By using Kubo's identity, Eq. (9) can be recast as

$$k(t) = \frac{i}{\hbar}\int_0^t dt{\rm Tr}\left\{\dot{\hat{\theta}}_R\hat{\mathcal{G}}(t)\hat{\theta}_R^\times\hat{\rho}_{\rm tot}^{\rm eq}\right\}, \quad (10)$$

where $\hat{\mathcal{G}}(t)$ is the Liouville space time propagator, which is evaluated from Eq. (8), and $\hat{\rho}_{\rm tot}^{\rm eq}(t)$ is the equilibrium density operator of the total system, which can be prepared by integrating Eq. (8) over sufficiently long time from the factorized initial state, $\hat{\rho}_{\rm tot}(-\infty) = \hat{\rho}(0)\otimes\hat{\rho}_{\rm B}^{\rm eq}$. In the HEOM formalism, the correlated (unfactorized) thermal equilibrium state can be set by using this steady state solution of the hierarchal elements.[65,66,76]

The right-hand side of Eq. (10) can be read as follows. At $t = 0$, the system in the thermal equilibrium state is excited

by the first interaction $\hat{\theta}_R^{\times}$ and propagated over the time t by $\hat{\mathcal{G}}(t)$. The first-order response function is then calculated from the expectation value of $\dot{\hat{\theta}}_R$. This is the numerical simulation for linear response measurement.[42,77] The rate constant is evaluated as $k_{\rm cnt} = k(+\infty)$.

III. RESULTS AND DISCUSSION

The system parameters adopted in this work are summarized in Table I and are representative of typical hydrogen-bridged systems. The system Hamiltonian is expressed in the energy eigenstate representation. Each eigenstate is labeled $|m, n\rangle$, where m and n represent an eigen-number of the PTR and RPV modes, respectively. This labeling is certainly meaningful for low lying vibrational states, while it can be problematic for higher energy excited states where the two modes can mix significantly. Furthermore, it enables us to clearly distinguish different paths of the proton transfer process. The procedure for labeling is defined in Appendix A. In order to numerically solve the HEOM, we employ the fourth-order Runge–Kutta method with a time step of $\delta t = 0.01/\omega_0$, where $\omega_0 = 110\ \text{cm}^{-1}$ is the lowest excitation energy of the system (see Appendix A). The depth and length of the hierarchy are chosen to be $N = 20$–50 and $K = 0$–1 with respect to different γ, and the lowest 12 eigenstates are utilized to describe the system. The accuracy of the calculation is maintained by increasing the values of N and K until numerical convergence.

A. Effective coupling strength and flux-flux correlation function

First, we note that when the inverse noise correlation time, γ, becomes large, the effective coupling strength increases, even if ζ is fixed, because the bath can interact with the system multiple times when the correlation time is short.[42] For the Drude SDF, Eq. (7), the effective coupling strength is expressed as $\zeta' = \zeta\gamma^2/(\gamma^2 + \omega_0^2)$. In the following, we employ ζ' to identify the pure non-Markovian effects and the pure non-perturbative effects separately.

Figure 3 illustrates the time evolution of the FFC function, $k(t)$, in (i) real time and (ii) Fourier space for the (a) weak, (b) intermediate, and (c) strong system–bath coupling cases for the fixed temperature $T = 300$ K ($\beta\hbar\omega_0 = 0.53$) and the inverse noise correlation time $\gamma = \omega_0$. In the present deep tunneling case, the time evolution of the FFC is highly oscillatory, as the system dynamics is characterized by the various excitation energies, in comparison with the semi-classical case described by a Brownian model with the LL interaction. In order to investigate the role of the transitions among the system states, we show the Fourier transformation of the signal in Fig. 3(ii). At $T = 300$ K ($\omega_{300\text{K}} \approx 200\ \text{cm}^{-1}$), the system is initially in the low energy states, yet high frequency transition peaks in Fig. 3(ii) are observed, due to the excitations induced by the operator θ_R.

Using Table II, we can identify all the transition peaks appearing in Figs. 3(ii–a)–3(ii–c). The peak labeled "A" corresponds to the transitions in the direct proton transfer (DPT) processes ($|0, n\rangle \to |1, n\rangle$ for $n = 1, 2, \ldots$), and the peak labeled "C" corresponds to the transitions in the excited proton transfer (EPT) processes ($|0, 0\rangle \to |2, 0\rangle$ and $|1, 0\rangle \to |2, 0\rangle$). Because the non-perturbative system–bath interaction can create a mixture of the PT and RPV vibrations, we observe the peaks that correspond to the PT-RPV transitions labeled "B1"($|1, n\rangle \to |0, n+1\rangle$) and "B2"($|0, n\rangle \to |1, n+1\rangle$). A schematic view of these three transition processes is presented in Fig. 2. It should be noted that these excitations decay toward the equilibrium state and the height and area of these transition peaks do not relate to the reaction rate that is determined near the equilibrium state. However, these profiles are helpful to investigate the dynamical aspect of the reaction processes.

In comparison with the results obtained from a Brownian model with the LL system–bath coupling,[30,41,42,78,79] the present EL coupling case exhibits highly oscillatory FFCs that are observed as the sharp peaks in Fig. 3(ii–c), even in the strong system–bath coupling case. This distinguished feature is due to the lack of the LL component, $q\sum_j g_j x_j$, for the PT mode in the EL system–bath coupling. Indeed, it has been shown that the SL interaction, $q^2\sum_j g_j x_j$, contributes to the vibrational dephasing (or frequency fluctuation) rather than the population relaxation.[59,80–84] Because the effect of the vibrational dephasing becomes larger for larger frequency modes (see Fig. 2), the peak profiles of the high frequency EPT modes ("C") are broadened, as illustrated in Fig. 3(ii–c), while the profiles of the low frequency DPT modes ("A") do not change even in the large system–bath coupling case. This indicates that the low frequency modes decay slower than the high frequency modes, as can be observed in Fig. 3(i).

TABLE I. System parameters.

Mass	M	100 amu
	m	1 amu
RPV mode	D_k	303 435 cm^{-1} Å^{-2}
	R_e	3.0 Å
Double well Morse	D	33 715 cm^{-1}
	r_e	1.0 Å
	α_0	2.0 Å

TABLE II. Eigen energy for the wave function $|m, n\rangle$ for the PTR and RPV eigenstates, m and n.

No.	$\lvert m, n\rangle$	Eigen energy, ω_0
1	$\lvert 0, 0\rangle$	0.00
2	$\lvert 1, 0\rangle$	1.00
3	$\lvert 0, 1\rangle$	3.61
4	$\lvert 1, 1\rangle$	4.81
5	$\lvert 0, 2\rangle$	7.26
6	$\lvert 1, 2\rangle$	8.63
7	$\lvert 2, 0\rangle$	10.52
8	$\lvert 0, 3\rangle$	10.94
9	$\lvert 1, 3\rangle$	12.44
10	$\lvert 0, 4\rangle$	14.53
11	$\lvert 2, 1\rangle$	14.79
12	$\lvert 1, 4\rangle$	16.25

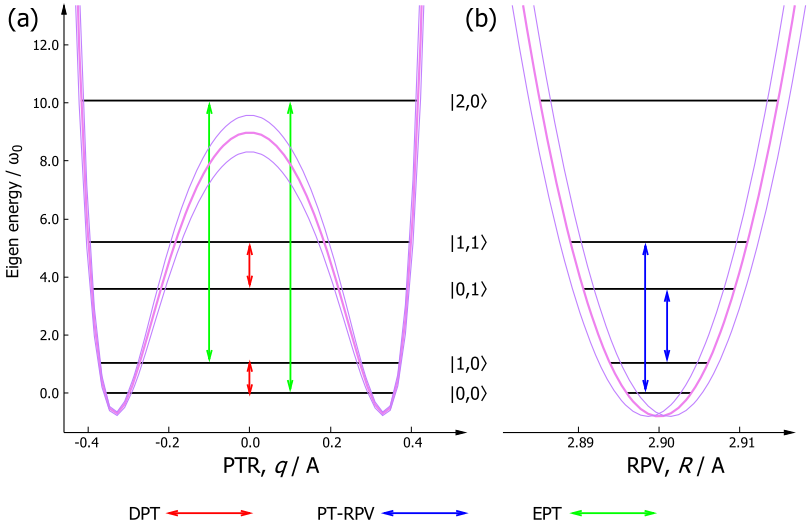

FIG. 2. The energy eigenstates $|m, n\rangle$ and the PES are schematically depicted in (a) the q direction for fixed R = 2.9 and (b) the R direction for fixed q = 0.35. The solid violet curve represents the unperturbed PES described by $U_0(\hat{q}, \hat{R})$, while the dotted and dashed curves represent the PES under the positive and negative bath perturbations. The EL system–bath interaction causes frequency modulation in the q direction and the shift of potential in the R direction. Thus, we observe vibrational dephasing in the PTR mode, while we observe population relaxation in the RPV mode. The direct proton transfer (DPT), PT-RPV, and excited proton transfer (EPT) transitions are illustrated by the red, blue, and green arrows, respectively.

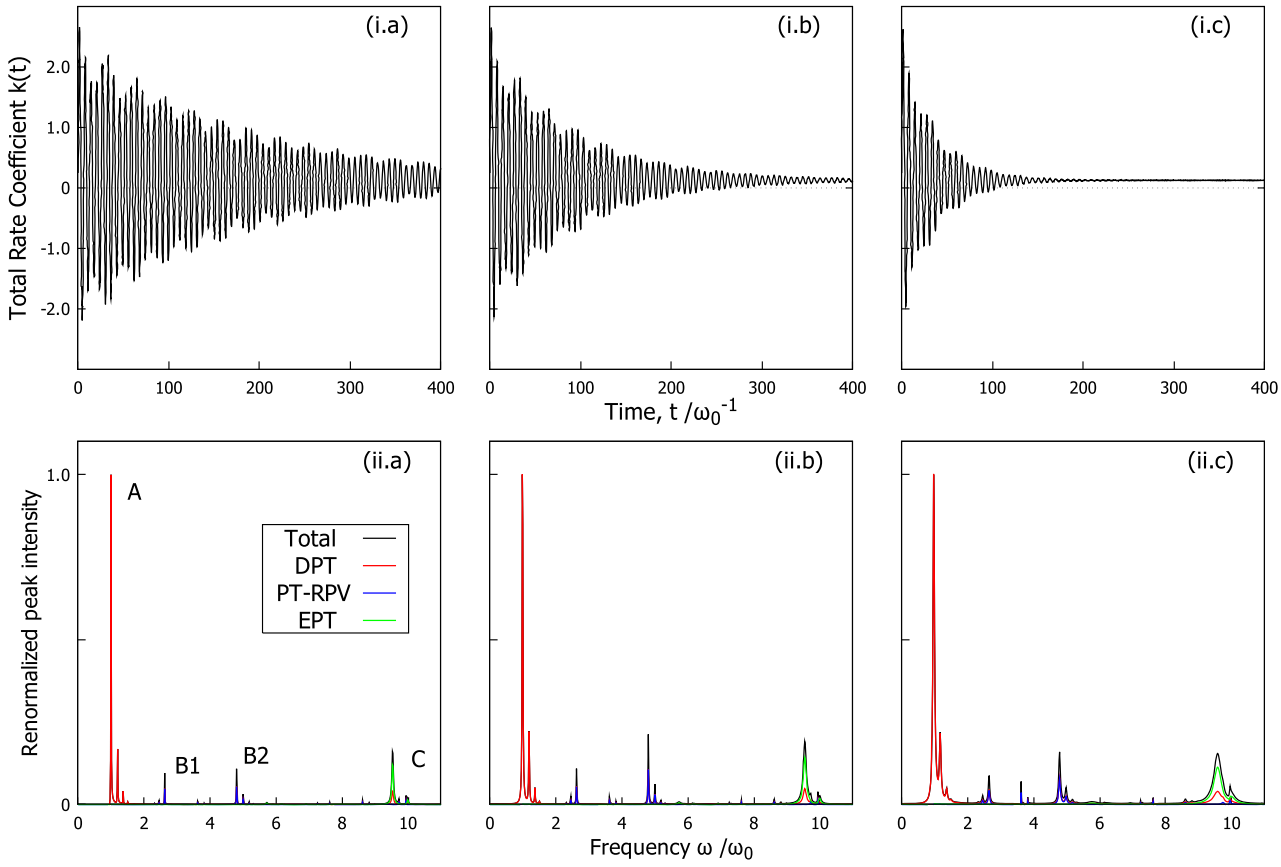

FIG. 3. The time evolutions of the flux–flux correlation (FFC) function, $k(t)$, are presented in the (i) real time and (ii) Fourier space for the (a) weak ($\zeta' = 0.1 \times 10^{-2}\omega_0$), (b) intermediate ($\zeta' = 0.2 \times 10^{-2}\omega_0$), and (c) strong ($\zeta' = 0.5 \times 10^{-2}\omega_0$) system–bath coupling cases, respectively. Here, we set T = 300 K and $\gamma = \omega_0$.

B. Temperature effects: Role of fluctuations

Next, we consider the temperature dependence of the rate constant k_{cnt} for a fixed inverse noise correlation time $\gamma = \omega_0$. In Fig. 4, we compare the rate constant as a function of coupling strength at different temperatures T: (a) 200 K ($\beta\hbar\omega_0 = 0.78$), (b) 300 K, and (c) 400 K ($\beta\hbar\omega_0 = 0.40$). The thermal excitation energy in this temperature regime is around 130–270 cm^{-1}. Thus, the DPT modes whose excitation energy is approximately $\omega = 110$–150 cm^{-1} are thermally well activated and provide the main contribution to the reaction rate. In order to illustrate this point, we separately plot the contribution from the DPT, PT-RPV, and EPT processes, which correspond to the peaks labeled "A," "B1" and "B2," and "C" in Fig. 3(ii), respectively (see Appendix B). Because the EL system–bath interaction creates transitions among the system states in a complex manner, DPT, EPT, and PT-RPV processes are highly entangled, as illustrated in the peaks in Fig. 3(ii). The EPT and PT-RPV contributions are relatively small regardless of the coupling strength due to the large excitation energies ($\omega = 500$–1000 cm^{-1}).

In the classical and quantum rate theory (Kramers theory) developed on the basis of the LL Brownian model, the turn-over feature from the energy controlled regime to the diffusion regime has been observed.[1–4,30,41,42,79] In the present case, while the reaction rate increases as ζ' increases in the small coupling strength region, we cannot observe the clear turn-over feature for large ζ'. This difference is due to the EL system–bath interaction. As discussed in Sec. II A, the major effects of the EL interaction with the PT mode are not population relaxation but vibrational dephasing. Thus, even for large ζ', the energy relaxation of the system states is slow, while non-dissipative vibrational modulation (or fluctuation) becomes larger. As a result, the reaction rate exhibits a plateau-like behavior for large ζ', while the rate predicted from the LL Brownian model decreases, which has been explained by the quantum version of the Kramers turn-over theory.[41,42]

The distinct difference between the LL Brownian case and the present case is observed in the high temperature case. In the framework of the LL Brownian theory, the reaction rate becomes larger for higher temperatures because the thermal activation process of the system enhances the reaction rate. In the present case, however, the reaction rate becomes smaller for higher temperatures. This is because the DPT process, which plays a dominant role in the PT reaction process, is suppressed due to the large vibrational dephasing effects arising from the thermal fluctuation, which depends on the temperature. For the EPT and PT-RPV processes, the excitation energies are much larger than the thermal excitation energy, and their contributions are small and do not change regardless of the temperature. In particular, when $T \to 0$ K, the excitation of the RPV mode will be suppressed, and the 2D system

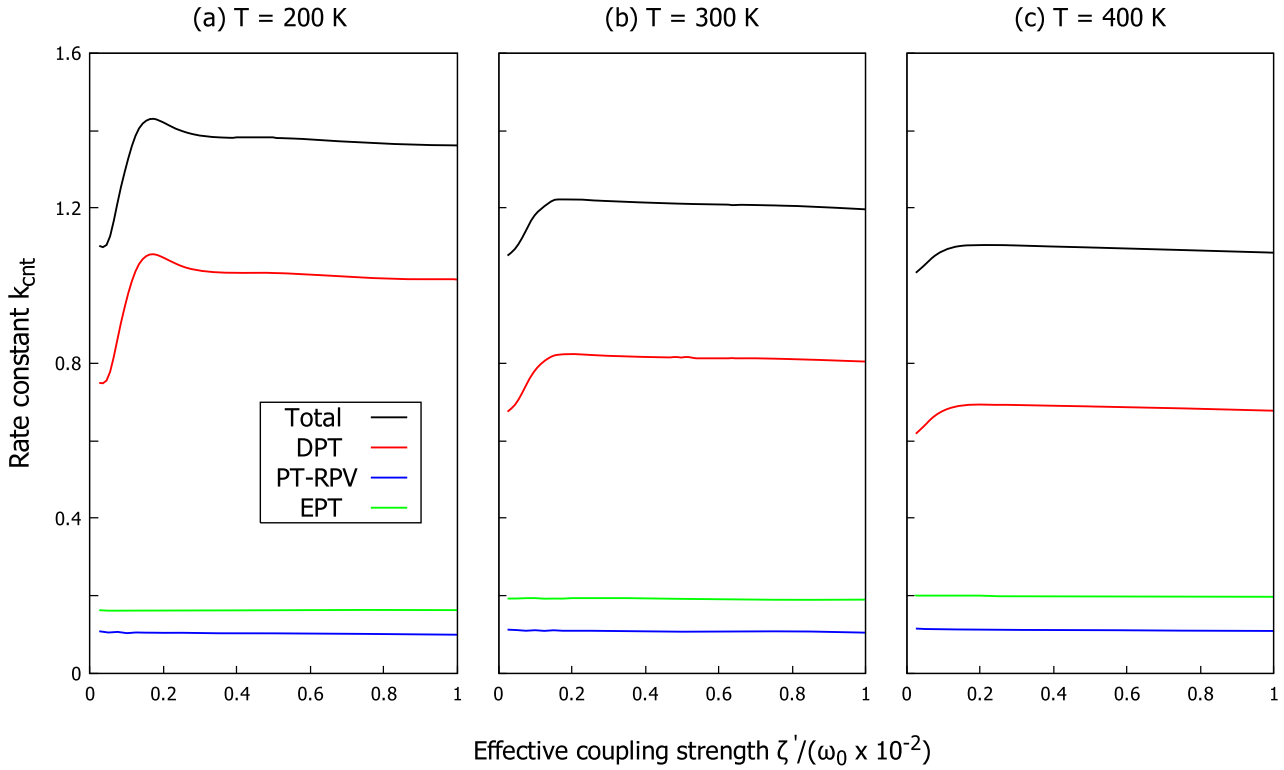

FIG. 4. The rate constants k_{cnt} are plotted as a function of the effective coupling strength ζ' at different temperatures T: (a) 200 K, (b) 300 K, and (c) 400 K. The contributions from the direct proton transfer (DPT), excited proton transfer (EPT), and PT-RPV processes are also depicted in the same colored curves as Fig. 3(ii). The inverse correlation time is $\gamma = \omega_0$. The abscissa has been scaled by a factor $0.01\omega_0$ only to improve the readability of the figure.

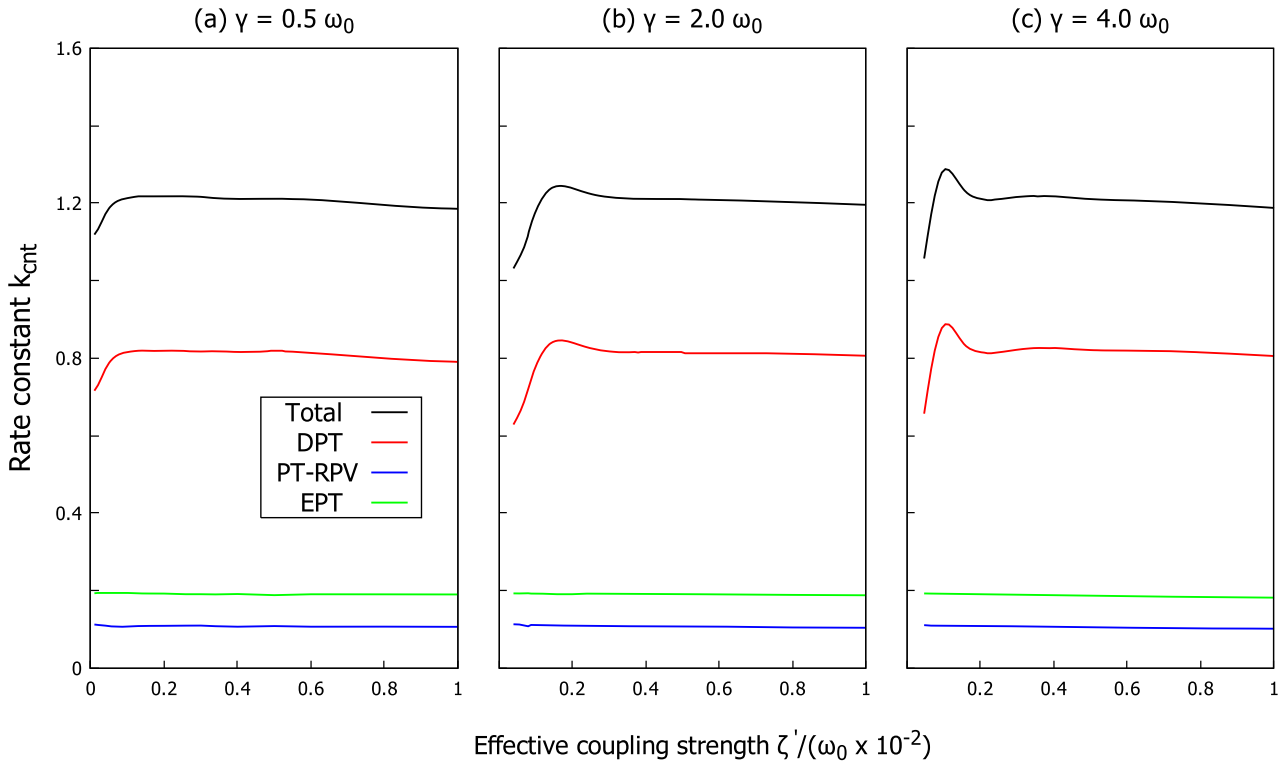

FIG. 5. Rate constant k_{cnt} as a function of ζ' for different inverse correlation time: (a) $\gamma = 0.5\omega_0$, (b) $2.0\omega_0$, and $4.0\omega_0$, at the fixed temperature $T = 300$ K. The case for $\gamma = 1.0\omega_0$ at $T = 300$ K is presented in Fig. 4(b). The contributions from the DPT, EPT, and PT-RPV processes are also depicted as the colored curves.

will be similar to the traditional 1D case (coupled to a heat bath at 0 K).

C. Non-Markovian and Markovian thermal effects

Finally, we consider the effect of the bath correlation time on the rate constant to investigate the role of non-Markovian and Markovian dynamics in the EL system–bath interaction. In Fig. 5, we present the rate constant as a function of ζ' for different γ. The case $\gamma = \omega_0$ is presented in Fig. 4(b). For the slow modulation case in Fig. 5(a), the reaction rate does not depend on the coupling strength except for the region with a very small ζ'. This is due to the slow bath modulation in the EL coupling case, in which the system evolves with time under the perturbed static potential.

For the intermediate modulation cases in Figs. 4(b) and 5(b), the rate increases with ζ' in the very weak coupling region. This is because the thermal activation process involved in the RPV–bath interaction, whose leading order agrees with the LL interaction (i.e., $R\sum_j g_j x_j$), takes place. This can be verified by changing the number of RPV states, n, involved in the calculation (see Appendix C). For a large ζ', vibrational dephasing, arising from the SL component of the EL interaction in the q direction, plays a dominant role instead of that from the LL component of the RPV mode in the R direction. Thus, we observe the turn-over feature for small ζ' as the quantum Kramers theory predicted, while the plateau-like feature of the reaction rate for large ζ' is observed due to the vibrational dephasing in the PTR mode. Regardless of γ, the contribution from the PT-RPV and EPT processes does not change because the vibrational dephasing plays a minor role in the relaxation process.

In the case of very fast modulation (the Markovian limit or the motional narrow limit) in Fig. 5(c), the maximum peak of the turn-over feature becomes more prominent due to the contribution from the higher RPV states in the relatively small coupling region. Regardless of the values of γ, the final value of the plateau-like feature is almost the same. This indicates that the vibrational dephasing effect arising from the SL component is determined by ζ', instead of ζ or γ.

IV. CONCLUSION

In this paper, we introduced a model described by a two-dimensional potential surface with a realistic EL system–bath interaction for the investigation of the proton transfer reaction rate. The distinct feature of the present mode arises from the EL interaction that is characterized by the SL system–bath interaction for the PTR mode and the LL system–bath interaction for the RPV mode. The LL interaction contributes to the population relaxation, while the SL interaction contributes to the vibrational dephasing. The interplay between the PTR mode and the RPV mode through the EL interaction exhibits distinctive features of the reaction process: in comparison with previous studies based on the Brownian LL model,

the turn-over feature of the reaction rate as a function of the system–bath coupling is suppressed because the vibrational dephasing does not contribute to the population relaxation so much. Most prominently, the reaction rate decreases when the temperature increases, which is the opposite to the prediction from the Kramers theory. While the lack of a linear coupling between the proton coordinate and the bath degrees of freedom might seem a strong assumption, we point out that, in our two-dimensional model, a significant potential $U(q, R)$ explicitly includes the dependence of the equilibrium position of the proton coordinate on the RPV coordinate, which is certainly a fundamental aspect to take into account to describe any proton transfer process.

Although the present investigations are limited to a specific model, we believe that the applicability of our findings to the exponential-linear system–bath coupling is wider as it includes most of the fundamental types of system–bath interactions. Proton-Coupled Electron Transfer (PCET) and Electron-Driven Proton Transfer (EDPT) mechanisms are also expected to show the types of system–bath interactions described here. Moreover, we can easily extend the present model to employ different system–bath coupling in the framework of the HEOM theory.

ACKNOWLEDGMENTS

The financial support from the Kyoto University Foundation is acknowledged. RB acknowledges the support of the University of Torino for the local research funding Grant No. BORR-RILO-18-01.

APPENDIX A: ENERGY EIGENSTATE REPRESENTATION OF THE PT SYSTEM

In this paper, we describe the system Hamiltonian and interaction function in terms of system eigenstates, calculated from the Schrödinger equation,

$$\left[-\frac{1}{2}\left\{\left(\frac{1}{m}+\frac{1}{M}\right)\frac{\partial^2}{\partial x^2}+\frac{2}{M}\frac{\partial^2}{\partial R^2}+\frac{2}{M}\frac{\partial^2}{\partial x \partial R}\right\}+U(\hat{q},\hat{R})\right]\Phi = E\Phi. \tag{A1}$$

The parameters we used are listed in Table I, based on the data of Ref. 38.

The quantum numbers m and n labeling the eigenstates of the system are determined from the number of nodes along the q and R directions, respectively. The eigen energies for the wave functions $|m, n\rangle$ are presented in Table II. The states $|0, n\rangle$ and $|1, n\rangle$ are the typical symmetric and asymmetric tunneling states, which are similar to those of the one-dimensional case. The state $|2, n\rangle$ and those that are mentioned above are the delocalized proton excited states. The energy of the first eigenstate $|0, 0\rangle$ is set to be zero. The characteristic frequency ω_0 is chosen to be the energy difference between states $|0, 0\rangle$ and $|1, 0\rangle$, which is near 110 cm^{-1}, and is used as the unit during the calculation.

APPENDIX B: PROJECTION OPERATOR

We consider the projection operator for the population of the acceptor state for the nth eigenstate of the RPV mode $\hat{\theta}_R^{(n)}$. The other

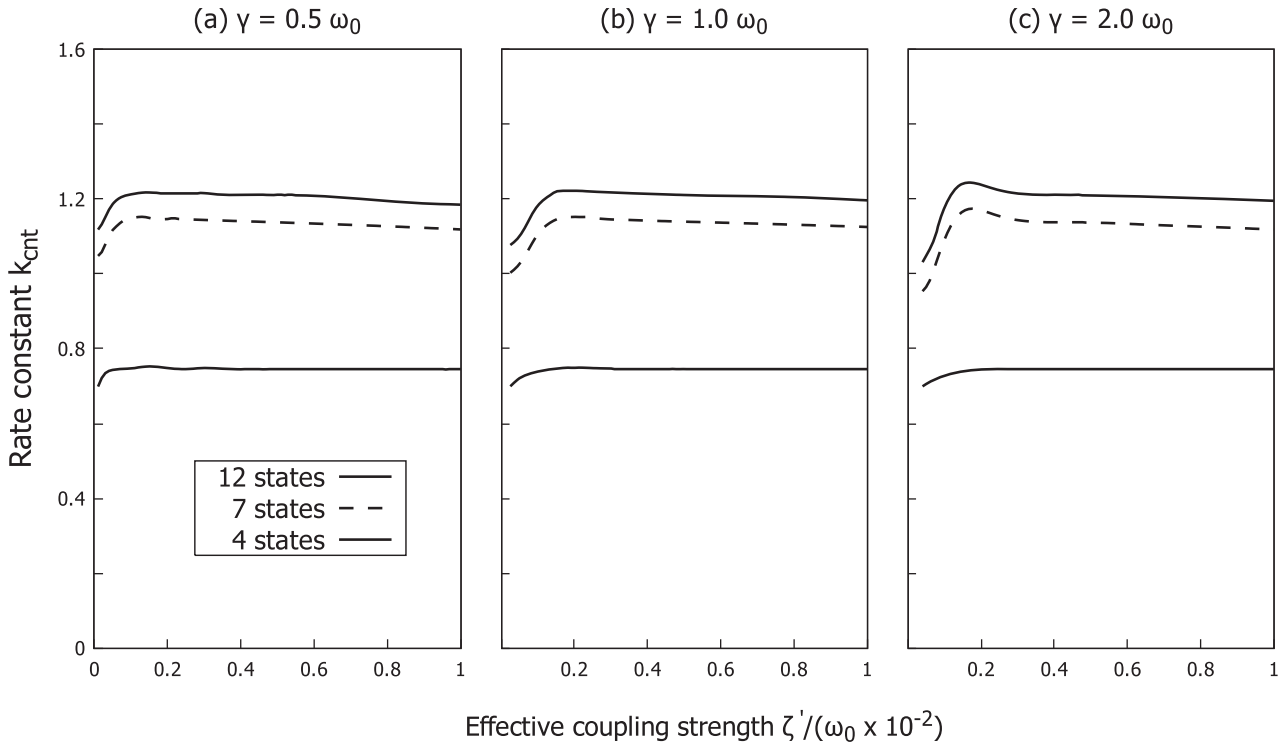

FIG. 6. Rate constant k_{cnt} for different RPV states described by n. The results for four, seven, and twelve eigenstates (the same condition in Fig. 5) are depicted in dashed, dotted, and solid curves. The temperature is fixed as T = 300 K.

projection operator for the donor state is given by $\hat{\theta}_L^{(n)} = 1 - \hat{\theta}_R^{(n)}$. The operator $\hat{\theta}_R^{(n)}$ is defined by

$$\hat{\theta}_R^{(n)} = \hat{h}(x)\,(\hat{\vartheta}^n + \hat{\vartheta}^E), \tag{B1}$$

where $\hat{h}(x)$ is the step function and $\hat{\vartheta}_n$ and $\hat{\vartheta}_E$ are the projection operators for $|m, n\rangle$ defined by

$$\hat{\vartheta}^{n'}\,|m,n\rangle = \begin{cases} |m,n\rangle & \text{if } m = 0 \text{ or } 1,\ n' = n \\ 0 & \text{if } m = 0 \text{ or } 1,\ n' \neq n \end{cases} \tag{B2}$$

and

$$\hat{\vartheta}^{E}\,|m,n\rangle = \begin{cases} 0 & \text{if } m = 0 \text{ or } 1 \\ |m,n\rangle & \text{if } m \geqq 2 \end{cases}. \tag{B3}$$

Using $\hat{\theta}_L^{(n)}$ and $\hat{\theta}_R^{(n)}$, we can separately evaluate the contribution from the donor and acceptor states for different n. Then, we can identify the contribution from DPT processes ($|0, n\rangle \to |1, n\rangle$ for $n = 1, 2, \ldots$), PT-RPV processes ($|1, n\rangle \to |0, n+1\rangle$ and $|0, n\rangle \to |1, n+1\rangle$), and EPT processes ($|0, 0\rangle \to |2, 0\rangle$ and $|1, 0\rangle \to |2, 0\rangle$).

APPENDIX C: ROLE OF THE RPV STATES

In order to investigate the role of the RPV states n, we calculate the reaction rate changing the number of system eigenstates. Figure 6 shows the calculated results of the reaction rate for the cases of the four ($n = 1$), seven ($n = 2$), and twelve ($n = 4$) eigenstates. When n is small, the result exhibits a similar profile as in Fig. 5(a). The rate calculated with four eigenstates is significantly smaller because the contribution from the EPT process is not involved. This RPV–bath LL interaction is prominent in the small ζ' region that leads the turn-over feature, as quantum Kramers theory predicted. In the large ζ' region, the vibrational dephasing, which is described by the SL interaction in the PTR mode, becomes dominant, and thus, the reaction rate shows the plateau-like feature.

DATA AVAILABILITY

The data that support the findings of this study are available from the corresponding author upon reasonable request.

REFERENCES

[1] P. G. Wolynes, Phys. Rev. Lett. **47**, 968 (1981).
[2] W. H. Miller, S. D. Schwartz, and J. W. Tromp, J. Chem. Phys. **79**, 4889 (1983).
[3] G. A. Voth, D. Chandler, and W. H. Miller, J. Chem. Phys. **91**, 7749 (1989).
[4] P. Hänggi, P. Talkner, and M. Borkovec, Rev. Mod. Phys. **62**, 251 (1990).
[5] A. L. Sobolewski, W. Domcke, and C. Hättig, Proc. Natl. Acad. Sci. U. S. A. **102**, 17903 (2005).
[6] Z. Lan, L. M. Frutos, A. L. Sobolewski, and W. Domcke, Proc. Natl. Acad. Sci. U. S. A. **105**, 12707 (2008).
[7] X. Liu, A. L. Sobolewski, R. Borrelli, and W. Domcke, Phys. Chem. Chem. Phys. **15**, 5957 (2013).
[8] Y. Cao, J. Eng, and T. J. Penfold, J. Phys. Chem. A **123**, 2640 (2019).
[9] Y. Kawashima and M. Tachikawa, J. Chem. Theory Comput. **10**, 153 (2014).
[10] G. A. Voth, J. Phys. Chem. **97**, 8365 (1993).
[11] S. R. Billeter and W. F. van Gunsteren, Comput. Phys. Commun. **107**, 61 (1997).
[12] D. Antoniou, M. R. Abolfath, and S. D. Schwartz, J. Chem. Phys. **121**, 6442 (2004).
[13] O. Pusuluk, T. Farrow, C. Deliduman, K. Burnett, and V. Vedral, Proc. R. Soc. A **474**, 20180037 (2018).
[14] P. Bamacký, Chem. Phys. **109**, 307 (1986).
[15] D. Antoniou and S. D. Schwartz, Proc. Natl. Acad. Sci. U. S. A. **94**, 12360 (1997).
[16] C. Hofmeister, P. B. Coto, and M. Thoss, J. Chem. Phys. **146**, 092317 (2017).
[17] A. V. Soudackov and S. Hammes-Schiffer, J. Chem. Phys. **143**, 194101 (2015).
[18] N. Došlić, J. Stare, and J. Mavri, Chem. Phys. **269**, 59 (2001).
[19] M. Basire, D. Borgis, and R. Vuilleumier, Phys. Chem. Chem. Phys. **15**, 12591 (2013).
[20] H. Wang, X. Sun, and W. H. Miller, J. Chem. Phys. **108**, 9726 (1998).
[21] M. W. Dzierlenga and S. D. Schwartz, J. Phys. Chem. Lett. **7**, 2591 (2016).
[22] V. L. Schramm and S. D. Schwartz, Biochemistry **57**, 3299 (2018).
[23] B. Salna, A. Benabbas, J. T. Sage, J. van Thor, and P. M. Champion, Nat. Chem. **8**, 874 (2016).
[24] D. C. Borgis, S. Lee, and J. T. Hynes, Chem. Phys. Lett. **162**, 19 (1989).
[25] D. Borgis and J. T. Hynes, Chem. Phys. **170**, 315 (1993).
[26] B. Peters, J. Chem. Theory Comput. **6**, 1447 (2010).
[27] D. Antoniou and S. D. Schwartz, J. Chem. Phys. **108**, 3620 (1998).
[28] L. O. Johannissen, N. S. Scrutton, and M. J. Sutcliffe, J. R. Soc., Interface **5**, 225 (2008).
[29] L. Chen and Q. Shi, J. Chem. Phys. **130**, 134505 (2009).
[30] Q. Shi, L. Zhu, and L. Chen, J. Chem. Phys. **135**, 044505 (2011).
[31] T. Meier, S. Petitgirard, S. Khandarkhaeva, and L. Dubrovinsky, Nat. Commun. **9**, 2766 (2018).
[32] Y. Masuda, Y. Mori, and K. Sakurai, J. Phys. Chem. A **117**, 10576 (2013).
[33] X.-Z. Li, B. Walker, and A. Michaelides, Proc. Natl. Acad. Sci. U. S. A. **108**, 6369 (2011).
[34] A. Ishizaki and G. R. Fleming, J. Chem. Phys. **130**, 234111 (2009).
[35] S. Sakamoto and Y. Tanimura, J. Phys. Chem. Lett. **8**, 5390 (2017).
[36] J. Zhu, S. Kais, P. Rebentrost, and A. Aspuru-Guzik, J. Phys. Chem. B **115**, 1531 (2011).
[37] R. Borrelli and M. F. Gelin, Sci. Rep. **7**, 9127 (2017).
[38] N. Sato and S. Iwata, J. Chem. Phys. **89**, 2932 (1988).
[39] D. Alfano, R. Borrelli, and A. Peluso, J. Phys. Chem. A **106**, 7018 (2002).
[40] E. R. Lippincott and R. Schroeder, J. Chem. Phys. **23**, 1099 (1955).
[41] Y. Tanimura and P. G. Wolynes, Phys. Rev. A **43**, 4131 (1991).
[42] Y. Tanimura and P. G. Wolynes, J. Chem. Phys. **96**, 8485 (1992).
[43] A. Kato and Y. Tanimura, J. Phys. Chem. B **117**, 13132 (2013).
[44] S. Daschakraborty, P. M. Kiefer, Y. Miller, Y. Motro, D. Pines, E. Pines, and J. T. Hynes, J. Phys. Chem. B **120**, 2281 (2016).
[45] P. F. Barbara, G. C. Walker, and T. P. Smith, Science **256**, 975 (1992).
[46] J. E. Bertie and Z. Lan, Appl. Spectrosc. **50**, 1047 (1996).
[47] S. Palese, S. Mukamel, R. J. D. Miller, and W. T. Lotshaw, J. Phys. Chem. **100**, 10380 (1996).
[48] M. Wendling, T. Pullerits, M. A. Przyjalgowski, S. I. E. Vulto, T. J. Aartsma, R. van Grondelle, and H. van Amerongen, J. Phys. Chem. B **104**, 5825 (2000).
[49] J. Adolphs and T. Renger, Biophys. J. **91**, 2778 (2006).
[50] C. Kreisbeck, T. Kramer, and A. Aspuru-Guzik, J. Phys. Chem. B **117**, 9380 (2013).
[51] C. Kreisbeck, T. Kramer, and A. Aspuru-Guzik, J. Chem. Theory Comput. **10**, 4045 (2014).
[52] M. K. Lee and D. F. Coker, J. Phys. Chem. Lett. **7**, 3171 (2016).
[53] S. Ueno and Y. Tanimura, J. Chem. Theory Comput. **16**, 2099 (2020).
[54] R. M. Lynden-Bell, Mol. Phys. **33**, 907 (1977).
[55] D. W. Oxtoby, D. Levesque, and J. J. Weis, J. Chem. Phys. **68**, 5528 (1978).
[56] S. Velsko and D. W. Oxtoby, J. Chem. Phys. **72**, 2260 (1980).
[57] S. Marks, P. A. Cornelius, and C. B. Harris, J. Chem. Phys. **73**, 3069 (1980).
[58] K. Okumura and Y. Tanimura, Phys. Rev. E **56**, 2747 (1997).
[59] A. Sakurai and Y. Tanimura, J. Phys. Chem. A **115**, 4009 (2011).
[60] B. Athokpam and S. G. Ramesh, J. Chem. Phys. **148**, 134503 (2018).
[61] Y. Tanimura and R. Kubo, J. Phys. Soc. Jpn. **58**, 101 (1989).
[62] Y. Tanimura, Phys. Rev. A **41**, 6676 (1990).

[63]A. Ishizaki and Y. Tanimura, J. Phys. Soc. Jpn. **74**, 3131 (2005).
[64]Y. Tanimura, J. Phys. Soc. Jpn. **75**, 082001 (2006).
[65]Y. Tanimura, J. Chem. Phys. **141**, 044114 (2014).
[66]Y. Tanimura, J. Chem. Phys. **142**, 144110 (2015).
[67]R. Borrelli, J. Chem. Phys. **150**, 234102 (2019).
[68]Y. Tanimura and S. Mukamel, J. Phys. Soc. Jpn. **63**, 66 (1994).
[69]M. Tanaka and Y. Tanimura, J. Phys. Soc. Jpn. **78**, 073802 (2009).
[70]T. Ikeda and Y. Tanimura, J. Chem. Theory Comput. **15**, 2517 (2019).
[71]Y. Tanimura, J. Chem. Phys. **137**, 22A550 (2012).
[72]H. Liu, L. Zhu, S. Bai, and Q. Shi, J. Chem. Phys. **140**, 134106 (2014).
[73]J. W. Tromp and W. H. Miller, Faraday Disscuss. Chem. Soc. **84**, 441 (1987).
[74]M. Topaler and N. Makri, J. Chem. Phys. **101**, 7500 (1994).
[75]T. Yamamoto, J. Chem. Phys. **33**, 281 (1960).
[76]L. Song and Q. Shi, J. Chem. Phys. **143**, 194106 (2015).
[77]R. Kubo, J. Phys. Soc. Jpn. **12**, 570 (1957).
[78]A. Ishizaki and Y. Tanimura, J. Chem. Phys. **123**, 014503 (2005).
[79]Y. Yan, M. Xu, Y. Liu, and Q. Shi, J. Chem. Phys. **150**, 234101 (2019).
[80]Y. Tanimura and A. Ishizaki, Acc. Chem. Res. **42**, 1270 (2009).
[81]T. Steffen and Y. Tanimura, J. Phys. Soc. Jpn. **69**, 3115 (2000).
[82]Y. Tanimura and T. Steffen, J. Phys. Soc. Jpn. **69**, 4095 (2000).
[83]T. Kato and Y. Tanimura, J. Chem. Phys. **117**, 6221 (2002).
[84]T. Kato and Y. Tanimura, J. Chem. Phys. **120**, 260 (2004).